Microscopic Modeling of the Dynamics of Frictional Adhesion in the Gecko Attachment System

ARTICLE *in* THE JOURNAL OF PHYSICAL CHEMISTRY B · APRIL 2009

Impact Factor: 3.3 · DOI: 10.1021/jp8067415 · Source: PubMed

4 AUTHORS, INCLUDING:

Tetsuo Yamaguchi
Kyushu University
20 PUBLICATIONS **228** CITATIONS
SEE PROFILE

Kellar Autumn
Lewis & Clark College
69 PUBLICATIONS **5,188** CITATIONS
SEE PROFILE

Costantino Creton
École Supérieure de Physique et de Chimie…
215 PUBLICATIONS **4,171** CITATIONS
SEE PROFILE

Microscopic Modeling of the Dynamics of Frictional Adhesion in the Gecko Attachment System†

Tetsuo Yamaguchi,§,‡ Nick Gravish,|| Kellar Autumn,|| and Costantino Creton*,‡

Laboratoire PPMD, CNRS-UPMC-ESPCI, 10 rue Vauquelin, 75231 Paris, Cedex 05, France and Department of Biology, Lewis and Clark College, Portland, Oregon 97219

Received: July 29, 2008; Revised Manuscript Received: September 26, 2008

We present a simple microscopic model describing the unique friction behavior of gecko setal arrays as they are dragged on smooth surfaces. Unlike other solids of high elastic modulus that do not stick under van der Waals forces alone, the gecko setal arrays do not require a compressive force to display a drag resistance but rather develop a tensile normal force when they are dragged (*J. Experim. Biol.* **2006**, *209*, 3569). We describe this unique behavior with a microscopic model involving curved beam structures at two length scales: at the spatula level, thousands of independent curved beams repeat detachment and reattachment, whereas at the seta level, the curved beam geometry of the seta induces a coupling between the frictional force and the adhesive force that depends on the angle of contact, therefore allowing easy release when the animal needs it. Our model accounts well for the dependence of the drag and adhesion forces on the drag velocity and can also explain macroscopic attachment/detachment cycles of the setal array.

Introduction

Most solids show normal or "Coulomb" friction when moved relative to one another. In this situation, a compressive load is necessary to measure a friction force, and the ratio between the tangential load and the normal load is called the friction coefficient and is usually a constant value smaller than 1.[2]

For soft materials however, the contact can be adhesive under van der Waals forces alone, and it is possible to observe frictional adhesion for polymer gels, rubbers, or soft adhesives. In this case, a tangential force is measured with a zero normal force or possibly with a negative normal force. Hence, the concept of friction coefficient does not make sense anymore, and a different description must be used. It is also worthwhile to note that for these very low modulus materials the motion parallel to the surface is never steady state but occurs by elastic instabilities at macroscopic scales.[3−6]

Gecko attachment systems made of multiple attachment points display frictional adhesion despite being made of hard materials.[1] Furthermore, the adhesive force increases with increasing drag velocity. This is a key condition to have a stable relative motion mechanism with an adhesive force (on the other hand, a decreasing friction with velocity would lead to a stick/slip motion).[7] Although several microscopic models have been proposed for the adhesive behavior of gecko attachment pads, they have focused either on the nature of the adhesive forces,[8] on the effect of contact splitting on the macroscopic adhesive force,[9] or more recently on explaining the angle dependence of the adhesive force.[10] None of these models has, however, addressed the dynamic frictional behavior, that is, how the gecko pad can simultaneously adhere and slip steadily on a surface. This property is important when the gecko wants to reattach its foot to a surface and apply a force to move forward or recover from a fall. The foot will not be immediately immobilized but rather will be dragged for a short distance with increasing frictional force. When the gecko wants then to lift its foot, it peels off the toe instead of dragging it on the surface. This costs very little energy.

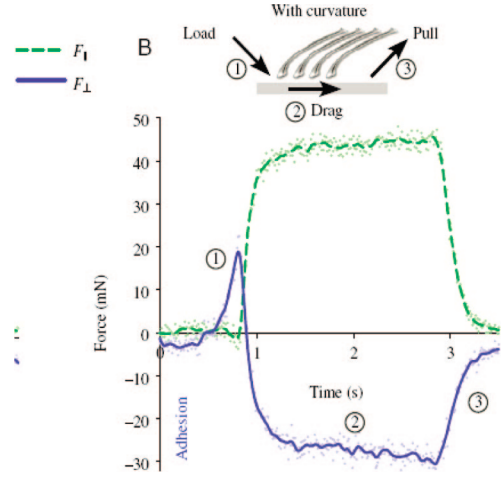

Figure 1. $F_{\parallel}$ (lateral force) and $F_{\perp}$ (normal force) versus time plot.[1]

We focus here on this attachment aspect of the gecko foot and propose a microscopic model describing the process of friction of a gecko setal array that is consistent with experimental observations and provides some interesting insights on the mechanisms by which such a frictional adhesion can work for materials with elastic moduli much larger than what is required for spontaneous adhesion.

General Picture

Isolated gecko setal arrays are known to exhibit very unique frictional/adhesion properties,[1] as shown in Figure 1. The key findings can be summarized as follows:

(A) Sliding motion can occur under negative normal force.

† Part of the "PGG (Pierre-Gilles de Gennes) Memorial Issue".

* To whom correspondence should be addressed. E-mail: costantino.creton@espci.fr.

‡ CNRS-UPMC-ESPCI.

§ Current address: Department of Applied Physics, The University of Tokyo, 7-3-1, Hongo, Bunkyo-Ku, Tokyo, 113-8656, Japan.

|| Lewis and Clark College.

10.1021/jp8067415 CCC: $40.75
Published on Web 12/02/2008

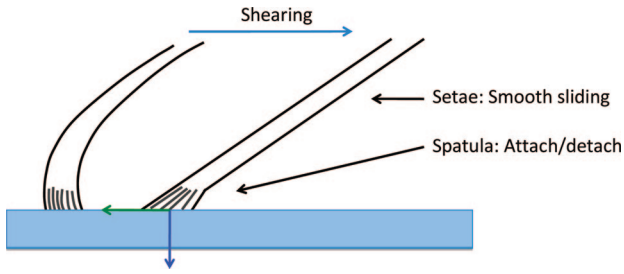

Figure 2. Schematic of the sliding motion of the gecko setae as we model it. Note that the setae straighten during forward motion but are unlikely to stretch.

(B) When a lateral displacement is applied at a fixed vertical displacement, both normal and lateral forces initially vary and even change their signs (compressive to tensile).

(C) The friction force then becomes almost constant in the steady sliding condition.

Properties A and B are very specific to this system, because a rigid sliding object normally separates from a substrate under negative loading and because the normal force does not vary so much (in some polymeric systems the normal stress changes under shear, but the effect is not so strong). Therefore, we have to answer the following questions: why is the sliding motion maintained under the negative loading condition, and how is the strong coupling between normal and lateral force generated in this system?

Moreover, although property C is less important than A or B, it implies that smooth sliding has to work under a negative loading. An unusual and difficult task, that is, that the system can sustain the negative loading and translate its center of gravity, requires new specific mechanisms.

Let us now address these questions. First, we define motion at two different length scales to make our discussion clear (see Figure 2).

•Mesoscopic motion: attachment/detachment of spatulae under negative loading, and their incoherent motions.

•Macroscopic motion: smooth sliding of the setae under negative loading.

We assume that the smaller structure such as spatulae works in a stick−slip manner but has a specific resticking mechanism from a detached conformation. Also, from experimental results,[1] a single seta seems to slide almost smoothly as shown in Figure 1. It is important to note that this classification has to be precisely made from experimental observations. However, we base our discussions on these assumptions.

In this paper, we discuss why the setae arrays exhibit such unique properties. In the following chapters, we discuss the attachment/detachment mechanisms by introducing the curved beam geometry and then propose an empirical rate-dependent detachment model for the tip of the spatulae based on the curved beam structure. We also try to explain the force space results of setal arrays by a simple model, and finally we summarize our results.

Mesoscopic Motion at the Spatula Level: Attachment/Detachment under Negative Loading and Rate-dependent Fracture. As we mentioned above, the sliding motion of the seta has to work under negative loading conditions. Here we propose an attachment/detachment mechanism for the individual spatula by modeling it as a curved beam. The attachment and detachment process of the beam, as we envision it, is schematically described in Figure 3. To be consistent with experimental results we specify the following rules: the beam is initially attached at one end to the seta and free at the other end. In this configuration, it is undeformed (a). When the spatula is pushed against the surface, it causes a compressive normal force (b). When the spatula is dragged along the surface with fixed normal displacement (c), it is progressively stretched until the adhesive contact fails (d) and the spatula jumps back to the original compressed position (e). In steady state sliding, the cycle (b−e) is repeated. This results in equations that are very similar to the molecular adsorption/desorption mechanisms proposed by Chernyak and Leonov[11] and discussed by Vorvolakos and Chaudhury,[12] but the mechanism is completely different: it is the mechanical attachment/detachment process working for even large objects through van der Waals forces, where thermal fluctuations are irrelevant, and as we will see later, this mechanism can maintain sliding friction even under negative loading.

When both ends are attached (during the drag stage), such a curved beam has a very useful mechanical property in this context, that is, the normal and lateral forces are coupled with each other.

In all generality, force-displacement relationships at the tip of a curved beam rigidly fixed at the other end can be expressed by the following equation.

$$\begin{bmatrix} f_{||} \\ f_{\perp} \end{bmatrix} = K \begin{bmatrix} d_{||} \\ d_{\perp} \end{bmatrix}, \quad K = \begin{bmatrix} K_{||,||} & K_{||,\perp} \\ K_{\perp,||} & K_{\perp,\perp} \end{bmatrix},$$

$$K_{||,||}, K_{\perp,\perp} > 0, \quad K_{||,\perp} = K_{\perp,||} < 0 \quad (1)$$

where $f_{||}$ and $f_{\perp}$ are the lateral and normal forces respectively, $d_{||}$ and $d_{\perp}$ are the lateral and normal displacements of the free tip of the curved beam, respectively, and K is the rigidity matrix to be determined from the detailed geometry of the beam.

As an illustrative example, we put the values in the rigidity matrix K for the parabolic curved beam (see Appendix 1), and imposed displacements at one end. The values are arbitrary in unit, but the procedure is similar to the experimental ones imposed to the seta, that is, a compressive vertical preload followed by a lateral displacement and do this at a given speed. We obtained the results of Figure 4.

$$K_{\text{spatulae}} = \begin{bmatrix} 5 & -3 \\ -3 & 2 \end{bmatrix} \quad (2)$$

$$(d_{||}, d_{\perp}) = (0,0) \xrightarrow{\text{load}} (0,1) \xrightarrow{\text{drag}} (3,1) \quad (3)$$

Figure 4 shows that even when we start from a compressed state, the normal force can become negative (tensile) as we pull one end laterally as long as the beam remains fixed at the other end. Of course this cannot occur indefinitely since once the beam becomes highly stretched, the adhesive contact with the surface will fail as described in Figure 3. It is important to note here that this normal−tangential coupling comes from the nonzero value of the off-diagonal element and also that it is generally observed for nonlinear beam structure. A more detailed calculation or optimization with a finite element method is addressed by Zhao et al. in a companion paper.[13]

If we now consider that N independent spatulae are undergoing this process in an uncorrelated manner, the macroscopic force will be N times the time-average force on a single spatula. To explain the velocity dependence of the force shown in Figure 5, we need to estimate a time on t_{on} and a time off t_{off}, that is, a characteristic time during which the beam is stretched and a

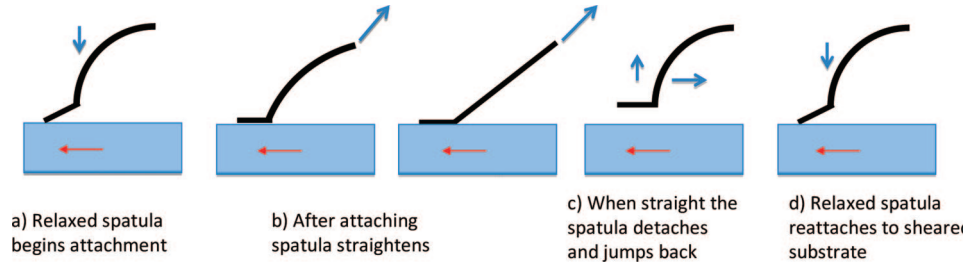

Figure 3. Attachment/detachment process of a single spatula.

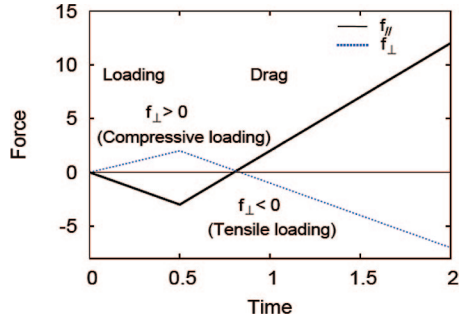

Figure 4. Schematic of the forces acting on the surface as a function of time during a compression (until $t = 0.5$ s) and lateral dragging motion (from 0.5 s to 2 s) occurring during the initial attachment of a curved beam. $f_\perp$ is the normal force, and $f_{||}$ is the tangential force.

characteristic resticking time during which the tip of the now unstretched or partially stretched spatula can reattach in a different position on the surface. This principle is similar to the molecular model of polymer friction.[11,12]

The stretching time will be roughly the distance required to fully stretch the beam divided by the sliding velocity. A spatula is about 1 μm long, 100 nm in diameter, and 200 nm apart. A reasonable stretching distance would therefore be on the order of 100 nm. Given the applied velocities in the experiments, t_{on} should be more than 100 μs (for $V < 1000$ μm/s). The resticking time on the other hand should not vary with velocity since it is related to the beam jumping back to its unstretched position. A reasonable estimate would be to take the resonant frequency of the spatula. The resonance frequency for a stiff cantilevered beam can be obtained from simple beam theory as:

$$\nu_R = 0.14\frac{D}{L^2}\sqrt{\frac{E}{\rho}} \tag{4}$$

Where D is the diameter, L is the length of the beam, E is its elastic modulus (1.5 GPa), and ρ its density ($\sim$1000 kg/m^3). Numerically, for spatulae that are 1 μm long, 100 nm in diameter, and 200 nm apart, one obtains $\nu_R = 34.3$ MHz, giving a t_{off} value on the order of 0.03 μs.

Therefore, in the experiment conditions we consider, the resticking time t_{off} is negligible, and the macroscopic tangential force $\bar{F}_{||}$ and normal force $\bar{F}_\perp$ can be calculated by the following equations.

$$\bar{F}_{||} = \frac{N}{t_{on} + t_{off}}\int_0^{t_{on}} f_{||}(t)\,dt \approx \frac{N}{t_{on}}\int_0^{t_{on}} f_{||}(t)\,dt \tag{5}$$

$$\bar{F}_\perp = \frac{N}{t_{on} + t_{off}}\int_0^{t_{on}} f_\perp(t)\,dt \approx \frac{N}{t_{on}}\int_0^{t_{on}} f_\perp(t)\,dt \tag{6}$$

The last but important point that remains to be discussed is the detachment criterion for the spatulae. If the detachment force was independent of t_{on}, it is simple to show that the time-averaged force could only decrease with increasing velocity, inconsistent with experimental data. This strongly suggests that the detachment criterion of the spatulae is not independent of t_{on} but increases as t_{on} decreases, that is, as the stretching rate of the spatulae increases. Let us examine possible physical pictures for the detachment criterion.

1. Viscoelastic Rupture Model. In the field of adhesion of elastomers, it is commonly found that the fracture energy of van der Waals contacts increases with increasing detachment velocity.[14−17] For elastomers, this effect is attributed to viscoelastic dissipative mechanisms acting close to the crack tip and increasing with velocity. The low velocity extrapolation is then the thermodynamic value of the work of adhesion. If we regard the fracture energy as the bond rupture energy for 1 spatula, one can then write

$$G_{vis}(V) = G_0\left\{1 + \left(\frac{V}{V^*}\right)^n\right\} \tag{7}$$

where $G_{vis}(V)$ is the bond rupture energy per single spatula, G_0 is the threshold adhesion energy at vanishingly low detachment rate, V^* is the characteristic velocity where dissipative processes become important during detachment, and n (0.3−0.6 in rubber) is an exponent depending on the mechanical properties of the material. The functional form of eq 7 is attractive since it produces the type of rate dependence that is experimentally observed.

2. Plastic Rupture Model. We discuss one possibility to describe the rate-dependent bond rupture criteria in 1. However, spatulae are not elastomers but rather are made of β-keratin, a stiff material analogous to a polymer glass that is not known to be viscoelastic. A clue comes from the considerable work done in the area of unlubricated friction of polymer glasses. Polymer glasses can slide relative to a smooth surface by the sliding of microscopic contact points due to asperities that can move by shearing a very localized nanometric layer that is deformed beyond the yield stress of the polymer.[18−21] In the case of the spatulae, the picture can then be that of the fracture of a single adhesive contact in mixed mode (shear and tension), involving local plasticity at the interface between the spatulae and the surface. An order of magnitude estimate of the plausibility of this mechanism comes from measurements on individual seta. Autumn et al. have shown that a single seta can sustain 200 μN in shear. If one assumes $\sim$500 spatulae per seta, this leads to a shear force of 0.4 μN/spatula, which is supported by an area of roughly 0.01 μm^2. The average shear stress to be

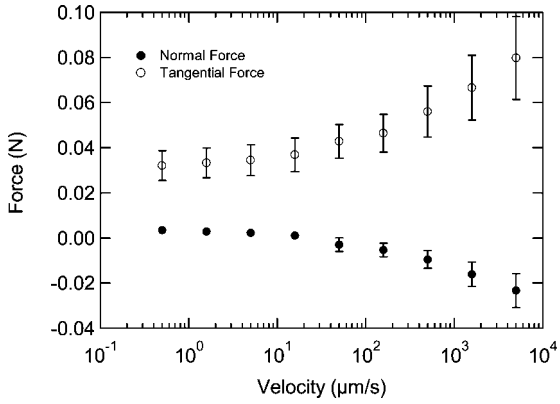

Figure 5. Nornal/Shear force vs drag velocity of a single seta.

transferred to the glass surface by each spatula is then of the order 40 μN/μm^2 or 40 MPa, clearly the order of magnitude of the yield stress of a molecular solid such as the β-keratin.

The bond rupture criteria of glassy polymers depends clearly on the strain rate that is applied and increases with strain rate in a different way as the viscoelastic model that is mentioned above. In the case of the debonding of the spatulae, one can then propose that the debonding will occur by plastic yielding of the adhesive patch. By applying the Eyring model, which describes thermally activated stick−slip in sliding friction, it could be written in the form of

$$G_{\mathrm{pl}}(V) = G_0 \sinh^{-1}\left(\frac{V}{V^*}\right) \tag{8}$$

Although it is the strain rate dependence of the yield stress that is classically described by the Eyring model,[22] we assume for simplicity that the energy of detachment of a contact G_{pl} is directly related to the yield stress, that is, the deformation at failure of the contact is not strain rate-dependent.

By using two types of rate-dependent bond rupture criteria and eqs 1, 5, and 6, we can obtain the expressions for the macroscopic forces. Detailed calculations are given in Appendix 2.

$$\bar{F}_{\parallel} \approx \frac{N}{2}\left\{f_{\parallel,1} + \sqrt{f_{\parallel,1}^2 + 2K_{\parallel,\parallel}G(V)}\right\} \tag{9}$$

and

$$\bar{F}_{\perp} \approx N\left\{f_{\perp,1} + \frac{K_{\perp,\parallel}}{2K_{\parallel,\parallel}}\left(-f_{\parallel,1} + \sqrt{f_{\parallel,1}^2 + 2K_{\parallel,\parallel}G(V)}\right)\right\} \tag{10}$$

Fitting of experimental data with the two models are shown in Figure 6. We can see that both rate-dependent rupture criteria fit experimental results well. It is important to note that the average normal force (i.e., time average of normal force of a single spatula) becomes negative even when we initially applied compressive displacement.

Macroscopic Motion at the Seta Level: Friction−Adhesion Coupling. Other than the above-mentioned steady state drag experiments, Autumn and co-workers have performed a series of experiments to study the transient frictional adhesion properties of setal arrays.[1] According to their results, when the setal arrays are pushed onto the glass substrate, the normal force becomes compressive, but the loading direction turns into negative (tensile) as they are pulled laterally. This means the friction and adhesion are coupled with each other even at this level (Figure 7).

This transient mechanical property can be understood with the same idea as that proposed for spatulae. First, we impose a linear force−displacement relation for setal arrays,

$$\begin{bmatrix} F_{\parallel} \\ F_{\perp} \end{bmatrix} = K_{\mathrm{seta}} \begin{bmatrix} D_{\parallel} \\ D_{\perp} \end{bmatrix} \tag{11}$$

The rigidity matrix of seta K_{seta} is assumed to have the following matrix elements, according to the parabolic curved beam model calculated in Appendix 1.

$$K_{\mathrm{seta}} \propto \begin{bmatrix} 5 & -3 \\ -3 & 2 \end{bmatrix} \tag{12}$$

We also put the displacement history for the setal arrays.

$$(D_{\parallel}, D_{\perp}) = (0,0) \xrightarrow{\text{load}} (4,7) \xrightarrow{\text{drag}} (6,7) \xrightarrow{\text{pull}} (0,0) \tag{13}$$

Here we assumed that there is some lateral slippage during the compression loading stage, causing the frictional force to relax. This is supported by the experimental observation that dragging the array against the curvature of the seta does give rise to regular friction and not frictional adhesion.

The calculated force space is shown in Figure 8.

It is important to note that there is some difference between the model structure and the actual one. By applying finite element calculations, it is possible to reproduce experimental force space or even optimize the structure to get desired frictional/adhesion properties, but this would be beyond the scope of the paper.

Discussion

Clearly, the model presented here still contains a certain number of assumptions that are not proven by experiment, but some of the features that we propose can have important implications for the design of future synthetic adhesives.

We feel that two key points deserve to be discussed. First, the reattachment mechanism of the individual spatula is the first important aspect. This is clearly a key microscopic feature holding the whole model together. In fact, as described in Figure 3, when the highly stretched and straight spatula is detached from the surface, it has to spring back to an equilibrium (bent) position and reattach instantly. The spring constant of the spatula may help in this mechanism since the slight compressive displacement imposed in the beginning means that the detached spatula springing back to equilibrium will touch the surface still in tension, and this will cause as slight dragging force that may be what is needed to instantly reattach. The fact that this mechanism is completely inactive in the other direction supports this idea.

The other important point is the rate dependence of the detachment force of the spatula. This feature is necessary to obtain a friction force increasing with velocity under adhesive conditions. This velocity dependence can only mean that the spatula is more stretched before detaching when it is stretched faster. Since there is no evidence of a viscoelastic or plastic behavior of the keratin making the spatulae, the most plausible idea is that the detachment involves dissipative mechanisms that

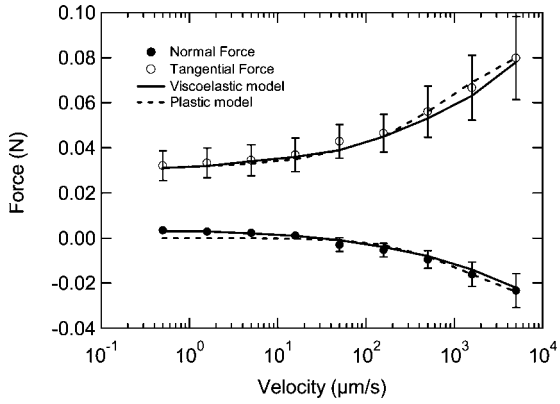

Figure 6. Comparison of experiment and theory (viscoelastic rupture model and plastic rupture model). The fitting parameters we used are $f_{\|,1} = 0$ N, $N(K_{\|,\|}G_0/2)^{1/2} = 0.03$ N, $V^* = 100$ μm/s, $n = 0.45$, $Nf_{\perp,1} = 0.02$ N, $[K^2_{\perp,\|}G_0/(2K_{\|,\|}f^2_{\perp,0})]^{1/2} = 0.8$ for the Viscoelastic rupture model (eq 7) and $f_{\perp,1} = 0$ N, $Nf_{\|,1}/2 = 0.03$ N, $2K_{\|,\|}G_0f^2_{\|,1} = 1$, $V^* = 600$ μm/s, $N K_{\perp,\|}f_{\|,1}/2K_{\|,\|} = -0.025$ N for the Plastic rupture model (eq 8).

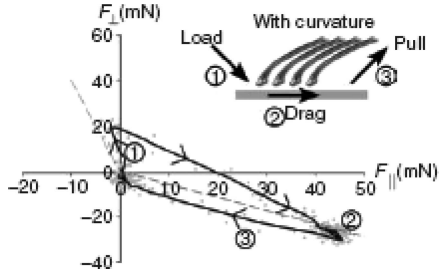

Figure 7. Force space measured by experiments.[1]

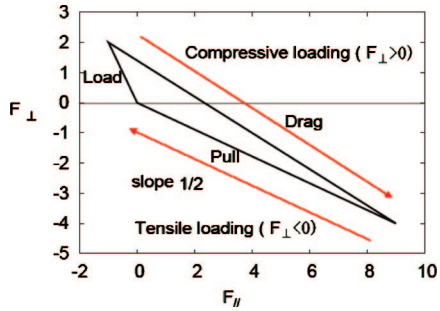

Figure 8. Calculated values of $F_\perp$ vs. $F_{\|}$ obtained from the curved beam model. The arrows represent the time variable during the cycle of loading/dragging/unloading realized experimentally and represented in Figure 7.

increase with separation velocity. Only microscopic experiments on a single spatula can resolve this point.

The final point worth discussing is the question of the stable friction (without stick/slip). This is a key feature that allows the gecko to run even when his feet are slipping. In normal Coulomb friction it is quite common to have this behavior, and it is related to the stiffness of the contact relative to the stiffness of the whole moving part. However, to obtain frictional adhesion with synthetic materials, the stiffness of the material itself has to be so low that it becomes impossible to have no stick/slip friction. The reason that this is possible in the setal arrays may be the hierarchical stiffness of the device. The stick−slip dissipative motion is confined to the spatula level, and the much stiffer seta level moves smoothly and stores a minimum amount of elastic energy during motion, thereby avoiding macroscopic slip. Such a hierarchical structure with a soft layer in contact with the surface and harder layer as backing has been shown to work in the much simpler pressure-sensitive-adhesives to optimize adhesive properties on weak substrates such as polyolefines[23] and may be the future of new, optimized adhesive materials.

Summary

In this paper, we have proposed a micromechanical model for the frictional adhesion mechanism observed for a setal array, taken from the foot of a gecko. This mechanism is remarkable since it allows steady state frictional motion under a tensile normal force, a mechanism that cannot yet be reproduced with our knowledge in synthetic materials.

The mechanism is based on a multiscale structure that combines a stick−slip motion at the spatula level with a curved beam structure that naturally couples an applied friction force with a normal force.

This attachment/detachment motion of the curved beam can maintain the macroscopic sliding motions under the negative loading, and we succeeded in providing qualitative explanations for the remarkable drag velocity dependence of the setal arrays that ensure a stable adhesion without catastrophic slippage. This feature is probably very useful to the gecko, which attaches probably more by frictional adhesion than by simple normal contact adhesion.

It is important to note that the frictional adhesion mechanism relies on two key features of the contact between the spatulae and the surface, which are the directionality of the contact (sticks when dragged in one direction but not in the other) and a rate dependence of the detachment energy of an individual spatula. Both features have not been yet proven by experiment but are consistent with experimental data.

We also found that the introduction of a curved beam structure can easily reproduce the transient frictional adhesion experiments of the setal arrays by coupling the parallel force with the normal force and is likely to be responsible as well for the easy detachment at the 30° angle observed for the setal arrays.

This model suggests then that the use of an asymmetric curved geometry for the structures will be a very useful feature to incorporate in synthetic gecko-like adhesives, which have so far mainly focused on straight pillars.

Appendices

Appendix 1.

Derivation of Rigidity Matrix for a Simple Curved Beam. In this appendix, we calculate the rigidity matrix of a simple curved beam shown in Figure A1. The torque M applied in the cross section $A(x, z)$ is expressed as

$$M(x) = -zF_{\|} - xF_{\perp} = -\frac{\sqrt{Lx}}{2}F_{\|} - xF_{\perp} \quad \text{(A1.1)}$$

where $F_{\|}$,$F_{\perp}$ are the applied horizontal and vertical force, respectively.

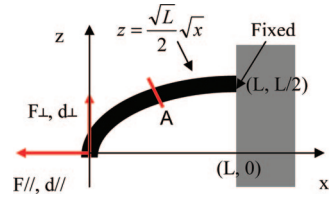

Figure A1

Strain energy can be calculated by the following equation

$$U = \frac{1}{2EI}\int_0^l ds M^2 = \frac{1}{2EI}\int_0^L dx\sqrt{1+\frac{L}{16x}}\left\{-\frac{\sqrt{Lx}}{2}F_{||} - xF_{\perp}\right\}^2 = \frac{L^3}{2EI}\left\{\frac{33}{1024}\sqrt{17} - \frac{1}{4096}\log(4+\sqrt{17})\right\}F_{||}^2 + \frac{L^3}{2EI}\left\{\frac{2077}{24576}\sqrt{17} + \frac{1}{32768}\log(4+\sqrt{17})\right\}F_{\perp}^2 + \frac{L^3}{2EI}\frac{1}{3840}\{391\sqrt{17}+1\}F_{||}F_{\perp} \quad \text{(A1.2)}$$

where L, E, and I are the length of the beam along x direction, Young's modulus, and the second moment of area, respectively.

From the strain energy function and the Castigliano's theorem, we get displacements.

$$D_{||} = \left.\frac{\partial U}{\partial F_{||}}\right|_{F_{||},F_{\perp}} = \frac{L^3}{2EI}\left\{\frac{33}{512}\sqrt{17} - \frac{1}{2048}\log(4+\sqrt{17})\right\}F_{||} + \frac{L^3}{2EI}\frac{1}{3840}\{391\sqrt{17}+1\}F_{\perp} \quad \text{(A1.3)}$$

and

$$D_{\perp} = \left.\frac{\partial U}{\partial F_{\perp}}\right|_{F_{||},F_{\perp}} = \frac{L^3}{2EI}\frac{1}{3840}\{391\sqrt{17}+1\}F_{||} + \frac{L^3}{2EI}\left\{\frac{2077}{12288}\sqrt{17} + \frac{1}{16384}\log(4+\sqrt{17})\right\}F_{\perp} \quad \text{(A1.4)}$$

To express A1.3 and A1.4 in a matrix form,

$$\begin{bmatrix} D_{||} \\ D_{\perp} \end{bmatrix} = \frac{L^3}{2EI} \times \begin{bmatrix} \frac{33\sqrt{17}}{512} - \frac{1}{2048}\log(4+\sqrt{17}) & \frac{1}{3840}(391\sqrt{17}+1) \\ \frac{1}{3840}(391\sqrt{17}+1) & \frac{2077}{12288}\sqrt{17} + \frac{1}{16384}\log(4+\sqrt{17}) \end{bmatrix} \times \begin{bmatrix} F_{||} \\ F_{\perp} \end{bmatrix} \quad \text{(A1.5)}$$

Finally, we obtain the force-displacement relationship.

$$\begin{bmatrix} F_{||} \\ F_{\perp} \end{bmatrix} = (2EI/L^3)\left/\left[\left\{\frac{33\sqrt{17}}{512} - \frac{1}{2048}\log(4+\sqrt{17})\right\} \times \left\{\frac{2077}{12288}\sqrt{17} + \frac{1}{16384}\log(4+\sqrt{17})\right\} - \left\{\frac{1}{3840}(391\sqrt{17}+1)\right\}^2\right] \times \begin{bmatrix} \frac{2077}{12288}\sqrt{17} + \frac{1}{16384}\log(4+\sqrt{17}) & -\frac{1}{3840}(391\sqrt{17}+1) \\ -\frac{1}{3840}(391\sqrt{17}+1) & \frac{33\sqrt{17}}{512} - \frac{1}{2048}\log(4+\sqrt{17}) \end{bmatrix} \begin{bmatrix} D_{||} \\ D_{\perp} \end{bmatrix} \quad \text{(A1.6)}$$

This model gives

$$K \propto \begin{bmatrix} 5 & -3 \\ -3 & 2 \end{bmatrix}$$

Appendix 2.

Calculation of the Normal/Frictional Force. Here we show the detailed calculation for the average force $\bar{F}_{||}$ and $\bar{F}_{\perp}$.

From Force-Displacement relationship (eq 1), we get expressions for lateral/normal force and elastic energy.

$$f_{||} = K_{||,||}d_{||} + K_{||,\perp}d_{\perp} \quad \text{(A2.1)}$$

$$f_{\perp} = K_{\perp,||}d_{||} + K_{\perp,\perp}d_{\perp} \quad \text{(A2.2)}$$

$$U = \frac{1}{2}[d_{||} \;\; d_{\perp}]\begin{bmatrix} f_{||} \\ f_{\perp} \end{bmatrix} = \frac{1}{2}[d_{||} \;\; d_{\perp}]\begin{bmatrix} K_{||,||} & K_{||,\perp} \\ K_{\perp,||} & K_{\perp,\perp} \end{bmatrix}\begin{bmatrix} d_{||} \\ d_{\perp} \end{bmatrix} \quad \text{(A2.3)}$$

Now we consider the situation where we initially impose the normal displacement $d_{\perp,0}$ (at this stage, the normal force is compressive), and then we drive the substrate laterally at a constant velocity V. As illustrated in Figure A2, we assume that the lateral force just after resticking (stage 1) is zero and that the spatula detaches from the substrate at the maximum extension (stage 2). The stored elastic energy is calculated as follows.

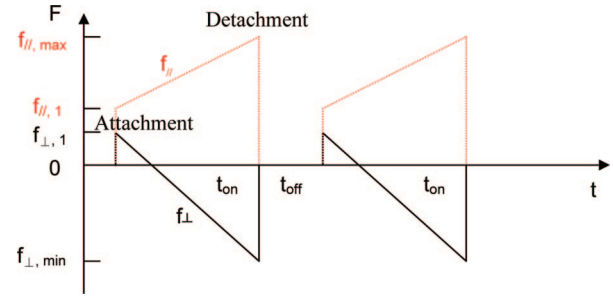

Figure A2

$$\Delta U = U(d_{||,2}, d_{\perp}) - U(d_{||,1}, d_{\perp}) = \frac{K_{||}}{2}(d_{||,2}^2 - d_{||,1}^2) + K_{||,\perp}(d_{||,2} - d_{||,1})d_{\perp} = \frac{K_{||,||}\Delta d_{||}^2}{2} + f_{||,1}\Delta d_{||} \quad \text{(A2.4)}$$

where $\Delta d_{||} = d_{||,2} - d_{||,1}$ is the lateral elongation of the spatula and $f_{||,1}$ is the lateral force just after resticking. We also assume the energy balance (i.e., stored elastic energy balances the dissipation),

$$\Delta U = G(V) \quad \text{(A2.5)}$$

then we obtain the following relation.

$$\Delta d_{||} = \frac{-f_{||,1} + \sqrt{f_{||,1}^2 + 2K_{||,||}G(V)}}{K_{||,||}} \quad \text{(A2.6)}$$

Equation A2.6 implies that the maximum stretch is dependent on the drag velocity.

From $t_{on} = \Delta d_{||}/V$ and eqs 5 and A2.6, we get

$$\bar{F}_{||} \cong \frac{N}{t_{on}} \int_0^{t_{on}} f_{||}(t)\, dt \cong N\frac{f_{||,1} + f_{||,max}}{2} = N\frac{2f_{||,1} + K_{||,||}\Delta d_{||}}{2} = \frac{N}{2}\{f_{||,1} + \sqrt{f_{||,1}^2 + 2K_{||,||}G(V)}\} \quad \text{(A2.7)}$$

and finally we obtain eq 9.

For the normal force, we can calculate in the same way using eqs 6 and A2.6,

$$\bar{F}_{\perp} \cong \frac{N}{t_{on}} \int_0^{t_{on}} f_{\perp}(t)\, dt = N\frac{f_{\perp,1} + f_{\perp,min}}{2} = N\left(f_{\perp,1} + \frac{K_{\perp,||}\Delta d_{||}}{2}\right) = N\left\{f_{\perp,1} + \frac{K_{\perp,||}}{K_{||,||}}(-f_{||,1} + \sqrt{f_{||,1}^2 + 2K_{||,||}G(V)}\right\} \quad \text{(A2.8)}$$

where $f_{\perp,1}$ and $f_{\perp,min}$ are initial and final (minimum) normal forces, respectively, and finally we get eq 10.

Acknowledgment. Part of this work was initiated during the sabbatical visit of Kellar Autumn at the ESPCI in the summer of 2007. We also thank Jacob Israelachvili and Hugh Brown for stimulating discussions.

References and Notes

(1) Autumn, K.; Dittmore, A.; Santos, D.; Spenko, M.; Cutkosky, M. *J. Experim. Biol.* **2006**, *209*, 3569.
(2) Persson, B. N. J. *Sliding Friction: Physical Principles and Applications*, 2nd ed; Springer: Berlin, Germany, 2000.
(3) Schallamach, A. *Wear* **1971**, *17*, 301.
(4) Baumberger, T.; Caroli, C.; Ronsin, O. *Phys. Rev. Lett.* **2002**, *88*, 0755091.
(5) Yamaguchi, T.; Doi, M. *Friction of polymer gels* 2008.
(6) Sosson, F.; Chateauminois, A.; Creton, C. *J. Polymer Sci. Part B* **2005**, *43*, 3316.
(7) Ciccotti, M.; Giorgini, B.; Barquins, M. *Int. J. Adhesion Adhesives* **1998**, *18*, 35.
(8) Autumn, K.; Sitti, M.; Liang, Y. C. A.; Peattie, A. M.; Hansen, W. R.; Sponberg, S.; Kenny, T. W.; Fearing, R.; Israelachvili, J. N.; Full, R. J. *Proc. Natl. Acad. Sci.* **2002**, *99*, 12252.
(9) Spolenak, R.; Gorb, S.; Arzt, E. *Acta Biomater.* **2005**, *1*, 5.
(10) Tian, Y.; Pesika, N.; Zeng, H.; Rosenberg, K.; Zhao, B.; McGuiggan, P.; Autumn, K.; Israelachvili, J. *Proc. Natl. Acad. Sci.* **2006**, *103*, 19320.
(11) Chernyak, Y. B.; Leonov, A. I. *Wear* **1986**, *108*, 105.
(12) Vorvolakos, K.; Chaudhury, M. K. *Langmuir* **2003**, *19*, 6778.
(13) Zhao, B.; Pesika, N.; Zeng, H.; Wei, Z.; Chen, Y.; Autumn, K.; Turner, K.; Israelachvili, J. Role of Tilted Adhesion Fibrils (setae) in the Adhesion and Locomotion of Gecko-like Systems, *J. Phys. Chem. B*, submitted for publication, 2008.
(14) Maugis, D.; Barquins, M. *J. Phys. D: Appl. Phys.* **1978**, *11*, 1989.
(15) Ahn, D.; Shull, K. R. *Langmuir* **1998**, *14*, 3637.
(16) Creton, C.; Brown, H. R.; Shull, K. R. *Macromolecules* **1994**, *27*, 3174.
(17) Persson, B. N. J.; Albohr, O.; Heinrich, G.; Ueba, H. *J. Phys.-Condensed Matter* **2005**, *17*, R1071.
(18) Bureau, L.; Caroli, C.; Baumberger, T. *Phys. Rev. Lett.* **2006**, 97.
(19) Bureau, L.; Baumberger, T.; Caroli, C. *Eur. Phys. J. E* **2006**, *19*, 163.
(20) Baumberger, T.; Berthoud, P.; Caroli, C. *Phys. Rev. B* **1999**, *60*, 3928.
(21) Berthoud, P.; Baumberger, T.; Sell, C. G.; Hiver, J.-M. *Phys. Rev. B* **1999**, *59*, 14313.
(22) Ward, I. M.; Sweeney, J. *An Introduction to the Mechanical Properties of Solid Polymers*, 2nd ed.; Wiley: Chichester, 2004.
(23) Carelli, C.; Déplace, F.; Boissonnet, L.; Creton, C. *J. Adhesion* **2007**, *83*, 491.

JP8067415